Applied Catalysis B: Environmental 90 (2009) 64–73

Contents lists available at ScienceDirect

Applied Catalysis B: Environmental

journal homepage: www.elsevier.com/locate/apcatb

Alternative bio-reduction synthesis method for the preparation of Au(AgAu)/SiO_2–Al_2O_3 catalysts: Oxidation and hydrogenation of CO

A.R. Vilchis-Nestor [a], M. Avalos-Borja [a,1], S.A. Gómez [b], José A. Hernández [b], A. Olivas [a], T.A. Zepeda [a,*]

[a] Centro de Nanociencias y Nanotecnología – Universidad Nacional Autónoma de México, Km. 107 Carretera Tijuana-Ensenada, 22800 Ensenada, B.C., Mexico
[b] Área de Ingeniería Química, Universidad Autónoma Metropolitana-Iztapalapa, Iztapalapa 09340, D.F., Mexico

ARTICLE INFO

Article history:
Received 24 December 2008
Received in revised form 15 February 2009
Accepted 19 February 2009
Available online 28 February 2009

Keywords:
CO hydrogenation
CO oxidation
CO methanation
PROX reaction
Nanostructured Au and Ag catalysts
Bio-reduction
Green nanochemistry

ABSTRACT

This paper describes the "one-step" bio-reduction synthesis method (using *sinensis* extract) for the preparation of Au and AgAu catalysts supported on SiO_2–Al_2O_3 (SA) material and their catalytic activity in the oxidation and hydrogenation of CO. For comparison the catalytic activity over reference Au/SA catalyst prepared by conventional deposition–precipitation (DP) method was included. The catalysts have been proved effectively as catalysts in the hydrogenation and oxidation of carbon monoxide in comparison with the sample prepared by DP procedure. The bimetallic AgAu/SA sample showed better behaviour in the CO oxidation, while in the CO hydrogenation reaction was the Au/SA monometallic sample which showed superior catalytic performance. Ours results showed that "one-step" bio-reduction synthesis method have proved to be uncomplicated, cost effectiveness and environmental friendly, that we expected this approach can be efficient to obtain nanostructured-supported Au and AgAu catalysts, with lower crystal size, homogeneous morphology and high catalytic performance and stability in the reactions involving the CO.

1. Introduction

The oxidation and hydrogenation of CO have been studied extensively [1,2]. Nowadays, the CO oxidation has attracted again the attention of numerous groups, due to the challenge obtaining novel and efficient catalysts for the oxidation of CO coming from the fossil fuels combustion [1,2]. Nevertheless, the CO hydrogenation is also as important as the CO oxidation reaction [3]. The potential application of the catalytic hydrogenation of CO to produce methane is in the purification of hydrogen streams from refineries, ethylene plants and hydrogen-rich reformate gases or alcohols [4]. In the last process, the CO hydrogenation (methanation) is a powerful effective means to reduce CO concentration to extremely low levels (<50 ppm), as those required in PEM fuel cell electrodes [5,6]. The use of CO methanation for the hydrogen-rich reformate purification instead of preferential oxidation (PROX) of CO, is related to that the PROX reaction requires the addition of oxygen (air) to the reformate-gas stream, which could reduced the hydrogen yield, or well it could affect the operation parameters during the fuel cell process [4]. Also the CO hydrogenation is employed during the ammonia synthesis to remove the CO traces from the H_2–N_2 mixture followed by water separation from the gas stream [1,7].

Although gold was long regarded as chemically inert because of its completely filled *d*-band [8], Haruta et al. showed that CO oxidation could be done at low temperature, provided the gold size particles formed on supports surface were very small [9–11]. Several reports have extensively reviewed the influence of type of support, pre-treatment conditions, the catalyst preparation method and the Au particle size on the catalytic response of gold catalysts in CO oxidation [12–25]. Grisel and Nieuwenhuys showed that the moderate metal–support interaction (MSI), the use of transition metal oxides as supports was proven to increase oxygen mobility in the oxidation reaction and induce electronic effects, improving thermal stability or decreasing the sintering of Au particles during the CO oxidation [16]. Then, the use of Au as catalysts for the CO oxidation has high potential; thus novel methodology to the preparation of Au catalysts basis is necessary.

On the other hand, after the first reported study by Bond and co-workers in 1960s, referent to the use of gold catalysts for reactions involving H_2 [8,17,18], only a little attention was paid to such reactions. The reason for this is because gold has completely filled

* Corresponding author. Tel.: +52 646 1744602x353; fax: +52 6461744603.
E-mail address: trino@icp.csic.es (T.A. Zepeda).
[1] On sabbatical leave at Division de Materiales Avanzados, IPICyT, San Luis Potosi, S.L.P. 78216 Mexico, Mexico.

0926-3373/$ – see front matter © 2009 Elsevier B.V. All rights reserved.
doi:10.1016/j.apcatb.2009.02.016

d-band and as a consequence it has a limited capacity to dissociate H_2 [8]. Still with this unfavourable electron configuration, renewed interest of gold catalysts for the hydrogenation of unsaturated molecules such as ketones, crotonaldehyde 1,3-butadiene, acrolein and unsaturated hydrocarbons, such as cyclohexane, benzene or biphenyl have emerged recently [19–25]. This is because their use may well be profitable when the factors controlling intra-molecular selectivity are more important than high HYD capability. However, very few reports on the hydrogenation of CO molecule over gold catalysts have been made [26,27]. The authors mentioned that gold could be a good candidate for the preparation of catalysts for CO hydrogenation. Also they showed that the type of support and the catalyst preparation method should have a strong effect on the catalytic performance during CO hydrogenation [26,27].

Summarizing, we can note that the use of gold has a high potential for the preparation of catalysts by deposition–precipitation (DP) method for both CO oxidation and hydrogenation reactions. Nevertheless, novel, cost-effective and "greener" approaches for the preparation of noble metal catalysts should be developed in order to transfer successfully this knowledge to the industry, because gold nanoparticles production remain expensive and/or involve hazardous chemicals. For example, during the last years, the biosynthesis of nanoparticles as an emerging high light of the intersection between nanotechnology and biotechnology has received increasing attention due to an ever-growing need to develop eco-friendly nanostructures synthesis procedures, with a superior control over the size and an excellent shape-selective arrangement [28].

Recently, the biosynthetic methods employing either biological micro-organism such as bacteria [29] and fungus [30] or plants extract [31] have emerged as a simple, low cost and eco-friendly approach to synthesize gold nanoparticles. In this sense, the bio-reduction method, using plants extract, for the fabrication of gold or gold nanoparticles in suspension-solution has been developed during the last years. Recently, we [31] found that a simple and efficient green nanochemistry approach is enough to prepare successfully gold and silver nanoparticles with a homogeneous size distribution in aqueous solution at room conditions, using a renewable and low cost biological reducing agent (*Camellia sinensis* plant extract), avoiding the presence of hazardous and toxic solvents or residues.

Within this scenario, the present work reports the potential use of novel green chemistry method for the easy one-step "green-synthesis" of supported monometallic Au and bimetallic AuAg catalysts on commercial SiO_2–Al_2O_3 material, using an eco-friendly and low cost synthesis involving the in situ bio-reduction of Au^{3+} and Ag^{1+} precursors by *C. sinensis* (green tea) extract. The synthesis and catalytic application of nanostructured Au/SiO_2–Al_2O_3 and AgAu/SiO_2–Al_2O_3 catalysts prepared by bio-reduction synthesis has not been reported. The samples were characterized by N_2 adsorption, DRX, TEM, DRS UV–vis and XPS methods. The Au/SiO_2–Al_2O_3 and AgAu/SiO_2–Al_2O_3 catalysts were tested in the CO oxidation and CO hydrogenation, both performed in a flow reactor at atmospheric pressure and in the 293–673 K temperature range.

2. Experimental

2.1. Synthesis of green Au and AgAu-supported catalysts

Monometallic Au and bimetallic AgAu-supported catalysts were prepared by incipient wetness impregnation of SiO_2–Al_2O_3 (SA) support. Commercial sodium-free SA material (Aldrich; with 380 $m^2\,g^{-1}$ of surface area, 7.1 nm of average pore size, 0.85 $cm^3\,g^{-1}$ of total pore volume and, 3.9 of point of zero charge) was used.

In the monometallic Au/SA sample preparation, 1 g of SA material was placed into a flask, and then 15 mL of an aqueous solution with the corresponding concentration of gold ($HAuCl_4{\cdot}3H_2O$, Aldrich, ACS reagent, purity of 99%) was added under stirred. Then 2 mL of *C. sinensis* extract were added to this solution, stirring vigorously for 48 h at room temperature. Then, the sample was dried at 373 K in air flow until the solvent was eliminated. Note: after few minutes that the *C. sinensis* extract was added, the solution tuned reddish-pink indicating the fast reduction of Au^{3+} ions.

The bimetallic AgAu/SA sample was prepared following a similar procedure as in the monometallic sample, but in this case, 7.5 mL of a solution with the corresponding concentration of gold was added to 1 g of SA material, followed by the addition of 1 mL of *C. sinensis* extract stirring constantly during 1 h. Then, 7.5 mL of a solution with the corresponding concentration of silver ($AgNO_3$, Aldrich, ACS reagent, purity of 99%) was added, following by the addition of 1 mL of *C. sinensis* extract, stirring vigorously for 48 h at room temperature. The Au/Ag atomic ratio was of 1. Then, the sample was dried at 373 K in air flow until the solvent was eliminated. Note: after few minutes that the *C. sinensis* extract was added, the solutions also change drastically in their coloration, indicating the reduction of both Au^{3+} and Ag^{1+} ions.

The reference Au/SA catalyst was prepared by conventional deposition–precipitation, adjusting the pH solution at 9 with a 3 M NH_4OH aqueous solution. The sample was filtered, washed with distilled water and dried at 373 K for 2 h. Then the sample was calcinated at 673 K for 3 h, the $[AuCl_4]^-$ species deposited on the support surface were easily decomposed with the formation of Cl_2 and/or HCl. The nominal Au loading of this sample was of 2.5 wt%.

The metal loading of both monometallic Au/SA and bimetallic AgAu/SA catalysts was determined by ICP (Table 1).

2.2. Characterization methods

2.2.1. N_2 adsorption–desorption isotherms

The nitrogen adsorption–desorption isotherms of the pure support and green catalysts were determined on an ASAP 2000 Micromeritics device. Prior to the experiments, the samples were degassed at 543 K in a vacuum for 5 h. The volume of adsorbed N_2 was normalized to standard temperature and pressure. Specific surface area (S_{BET}) was calculated by the BET equation applied to the range of relative pressures $0.05 < P/P^0 < 0.30$. The average pore diameter (APD) was calculated by applying the Barret–Joyner–Halenda method (BJH) to the desorption branches of the N_2 isotherms. The cumulative pore volume was obtained from the isotherms at $P/P^0 = 0.99$.

2.2.2. X-ray diffraction

The X-ray patterns of the pure support and green catalyst in the 2θ range of 10–60° at a step of 0.02° were recorded on a Philips spectrometer model X'pert, using a Cu Kα radiation ($\lambda = 0.1541$ nm).

2.2.3. Transmission electron microscopy (TEM)

TEM studies and SAED (selected area electron diffraction) technique were carried out using a JEOL 2010 microscope operating at 200 kV accelerating voltage. The catalysts were

Table 1
Labeling and chemical composition of pure support and catalysts.

Sample	Labeling	Au (wt%)[a]	Ag (wt%)[a]	Al_2O_3 (wt%)[a]
SiO_2–Al_2O_3	SA	–	–	26
Au/SiO_2–Al_2O_3	Au/SA	2.05	–	25.2
AgAu/SiO_2–Al_2O_3	AgAu/SA	0.88	1.32	24.6

[a] Au and Al_2O_3 wt% was derived from chemical analysis (ICP).

ground into a fine powder and then dispersed ultrasonically in 2-propanol at room temperature. A drop of the suspension was then put on a carbon-coated Cu grid. At least 10 representative images were taken for each sample. In order to obtain statistically consistent information, the length of ca. 500 particles was measured. Particle size distributions were obtained by counting more than ca. 500 particles for each sample. Particle size diameters were calculated with the equation $d_{avg} = \sum(n_i d_i)/\sum n_i$, where n_i is the number of particles of diameter d_i.

2.2.4. UV–vis diffuse reflectance spectroscopy

UV–vis diffuse reflectance spectra (DRS UV–vis) of the catalysts were recorded using a Cary 5_E spectrophotometer (Varian) with a specially designed Praying Mantis diffuse reflection cell (Harrick Scientific) for in situ measurements. All spectra were recorded after heating the samples at 523 K in He flow for 1 h. The spectrum of the pure support was subtracted from the spectrum of the catalyst.

2.2.5. X-ray photoelectron spectroscopy (XPS)

X-ray photoelectron spectra of catalysts were measured in a VG Escalab 200R spectrometer equipped with a hemispherical electron analyzer and a Mg Kα ($h\nu$ = 1253.6 eV) X-ray source. Samples were first placed in a copper holder mounted on a sample-rod in the pre-treatment chamber of the spectrometer and then outgassed at 403 K for 1 h before transfer to the analysis chamber. All samples were outgassed at 10^{-5} mbar and then transferred to the ion-pumped analysis chamber, where residual pressure was kept below 7×10^{-9} mbar during data acquisition. The binding energies (BE) were referenced to the C 1s peak (284.9 eV) to account for the charging effects. The areas of the peaks were computed after fitting the experimental spectra to Gaussian/Lorentzian curves and removal of the background (Shirley function). Surface atomic ratios were calculated from the peak area ratios normalized by the corresponding atomic sensitivity factors.

2.3. Catalytic activity measurements

Previous to the catalytic experiments, the reference sample (Au/SA catalyst prepared by conventional DP method) was reduced/activated in situ under a flow of hydrogen of 60 mL min^{-1} at atmospheric pressure and 623 K for 3 h. Both bio-reduction Au/SA and AgAu/SA samples, previous to the catalytic test, were calcined at 463 K for 1 h in static air, in order to remove the organic compound deposited from bio-reduction *sinensis* extract solution.

2.3.1. Oxidation of CO

CO oxidation was carried out in a bed quartz micro-reactor connected on-line to a GC Shimadzu 12-A (5-A and Porapack Q) with two packed columns equipped with a TCD. 150 mg of the catalysts were introduced into the micro-reactor, and the sample was then contacted with a gas mixture (1, 0.5 and 98.5% (v/v) of CO, O_2 and N_2, respectively, 100 mL/min of total flow). The activities of gold catalysts were evaluated at atmospheric pressure and working in a 293–673 K temperature range with a heating rate of 3 K min^{-1}.

2.3.2. Hydrogenation of CO

CO hydrogenation was carried out in a bed quartz micro-reactor connected on-line to a GC Shimadzu 12-A (5-A and Porapack Q) with two packed columns equipped with a TCD and a Hidden CG-mass spectrometer model HAL RC 301. 150 mg of the catalysts were introduced into the micro-reactor, and the sample was then contacted with a gas mixture (1, 50 and 49% (v/v) of CO, H_2 and N_2, respectively, 100 mL/min of total flow). The activities of gold catalysts were evaluated at atmospheric pressure and working in a 293–673 K temperature range with a heating rate of 3 K min^{-1}.

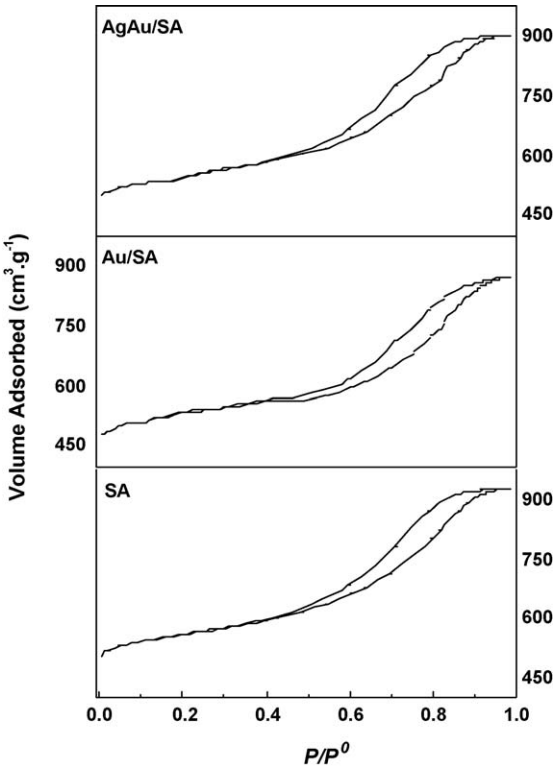

Fig. 1. Nitrogen adsorption–desorption isotherms of pure support and catalysts.

3. Results and discussion

3.1. 3.1 N_2 adsorption–desorption isotherms

The nitrogen adsorption isotherms of the support and catalysts are shown in Fig. 1. In all cases the isotherms correspond to type IV, according to the IUPAC classification [32], with a sharp step at intermediate relative pressures. All samples showed a capillary condensation steps about 0.80–0.85 that is due to textural inter-particle mesoporosity or macroporosity. The appreciable hysteresis loops of samples belong to type H_2, which are characteristic of the pores with non-uniform size and shape [33].

The specific area, average pore diameter, average pore volume (V_p) and normalized S_{BET} values of the support and catalysts are listed in Table 2. The pure SA support has a S_{BET} value of 380 $m^2\ g^{-1}$, APD of 7.1 nm and V_p 0.87 $cm^3\ g^{-1}$. A comparison of the S_{BET} value of the pure support with the catalysts indicates that S_{BET} values decreased upon the incorporation of noble metals (Table 2). Since the bimetallic AgAu/SA sample shows a higher S_{BET} value than the monometallic Au/SA sample (Table 2).

In general, we can say that the APD of the catalysts remains virtually the same as the values observed in the pure supports. However, we can also observe a light decrement in the V_p value of the catalysts in comparison with the pure support. The possible

Table 2
Textural properties of pure support and catalysts.

Sample	S_{BET} ($m^2\ g^{-1}$)	APD (nm)	V_p ($cm^3\ g^{-1}$)	NS_{BET}[a]
SA	380	7.1	0.87	1
Au/SA	340	7.0	0.78	0.85
AgAu/SA	369	7.1	0.84	0.95

[a] NS_{BET}: normalized S_{BET} value.

explanation is that the larger supported particles are blocking some porosity of the SA material, as indicates the S_{BET} values. We could therefore conclude that the structural parameters of the support are preserved after the deposition of gold particles. To clarify this argument, we could take the normalized S_{BET} values calculated using an equation proposed by Vradman et al. [34] and discussed based on our previous results [35]:

$$NS_{BET} = \frac{S_{BET\ of\ catalyst}}{(1-y) \times S_{BET\ of\ support}}$$

where NS_{BET} is normalized S_{BET} and y is the weight fraction of the supported phases. Table 2 shows the normalized values of the specific surface area (NS_{BET}) of the catalysts. The NS_{BET} value of the bimetallic catalysts is very close to 1, while the NS_{BET} value of the monometallic samples is 0.86. This observation indicates that no important changes occur in the textural parameters of the support. Nevertheless, these results are indicative that the active phase in the bimetallic sample is principally localized on the external surface (from NS_{BET} value around 1), while in the monometallic sample the NS_{BET} value of 0.85 could be an indicative that some fraction of the active phase is localized into of the pore support blocking some SA nanoporosity, but the majority of the active phase could be localized on the external surface.

3.2. X-ray diffraction and transmission electron microscopy

The wide-angle X-ray patterns of the support and catalysts are shown in Fig. 2. The X-ray patterns of the both support and catalysts exhibited a broad line between 20° and 30°, which was attributed to the siliceous amorphous phase [36]. As it was expected, we can note the absence of diffractions peaks in the pure support. In contrast, the catalysts showed two diffraction peaks at 38.1° and 44.6°. The presence of those two XRD signals indicate the presence of Au^0 phase, characteristic of the crystalline planes (1 1 1) and (2 0 0) of metallic gold, respectively [37,38]. However, the diffraction peaks of Ag^0 appear approximately in the same position than those diffraction peaks of Au^0. Therefore, in the case of the bimetallic catalyst, we cannot assign directly the diffraction peaks of the metallic Au^0 or Ag^0. Nevertheless, we can note the absence of silver nitrate diffractions peaks, and then we could assume that the two diffractions peaks observed in the bimetallic sample are composed by both Au^0 and Ag^0 signals. We can note that the width and the intensity of those diffractions peaks (38.1° and 44.6°) decreases in the bimetallic sample, in comparison with the monometallic sample. Then, we could assume that the presence of Ag favours the dispersion of metallic species. To verify this we calculate the average particle size using the Scherrer-equation. The average particle size in the monometallic sample, which corresponds to 2θ values of 38.1° and 44.6°, were of 11.5 and 10.3 nm, respectively, while in the case of the bimetallic sample the average particle size was 8.4 and 9.6 nm, respectively. We can note that the presence of silver on gold has an effect on the gold particle size.

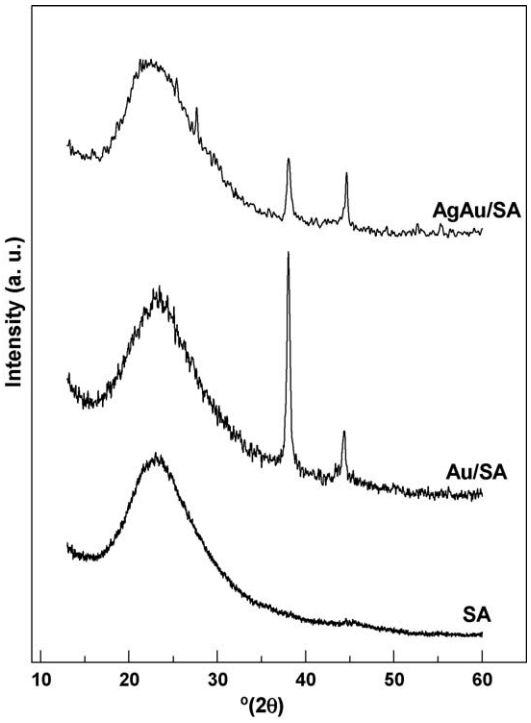

Fig. 2. X-ray diffraction corresponds to the support and catalysts.

An additional reflection peak was observed in the bimetallic sample centred at 27.6°, being characteristic of the presence of AgCl with the crystalline plane (1 1 1) [39]. The formation of AgCl phase is unavoidable due to the high reactivity of the silver with chlorine present in the gold precursor ($HAuCl_4$).

TEM analysis was carried out in order to study the average particle size of catalysts synthesized by bio-reduction method. Representative TEM images and their diffraction patterns for the Au/SA and AgAu/SA catalysts are shown in Figs. 3 and 4, respectively. We can note that the morphology in both samples is similar, but the bimetallic AgAu/SA sample has higher regular morphologic, in comparison with the monometallic sample. The SAED pattern in Fig. 3(b) revealed the presence of diffraction rings with d-spacing of 2.301, 2.039, 1.442 and 1.23 Å, these are associated (1 1 1), (2 0 0), (2 2 0) and (3 1 1) planes of gold, labelled in Fig. 3(b) as 1, 2, 3 and 4, respectively. On the other hand bimetallic AgAu nanoparticles are also crystalline, and have a more uniform size and morphology, as is indicated in the TEM image and in the electron pattern of diffraction of this sample (Fig. 4(a)). The indexed diffraction spots of this sample are assigned to {1 1 1} and {2 0 0} planes of an fcc structure of both, Au and Ag particles.

Particle size distribution corresponding to monometallic Au/SA and bimetallic AgAu/SA catalyst is shown in Fig. 5(a) and (b), respectively. In both samples, we can note that most of the metallic particles are centred between 1.5 and 6.5 nm, observing the higher peak in the particle distribution centred at 4.5 nm. In these figures, we can note that the bimetallic AgAu/SA sample have higher amount of Au particles of size lower that 4.5 nm, in comparison with the monometallic Au/SA sample. Nevertheless, several differences between the XRD and TEM results are observed. These can be explained by the fact, that the two methods used provide different information about the particle size. The XRD analysis gives a 'volume average measurement' and refers to the size of crystallites of the material. In contrast, the TEM measurement provides real information of the size and size distributions of particles, principally those particles in the size interval that cannot be detected by XRD. Finally, we can confirm the observation made in XRD discussion, that the silver and gold mixture result in metallic particles with a sharp size distribution, regular morphology and higher dispersion than in the case of monometallic catalyst (Figs. 3–5).

3.3. UV–vis diffuse reflectance spectroscopy

Fig. 6 shows the electronic spectra of catalysts after the subtraction from the DRS UV–vis spectrum of the support. Both electronic spectra have an intense band at 518 nm. The presence of this absorption band is attributed to the surface plasmon resonance of both Au and AuAg nanoparticles [40]. The plasmon band is due to the effect of collective oscillations of the free

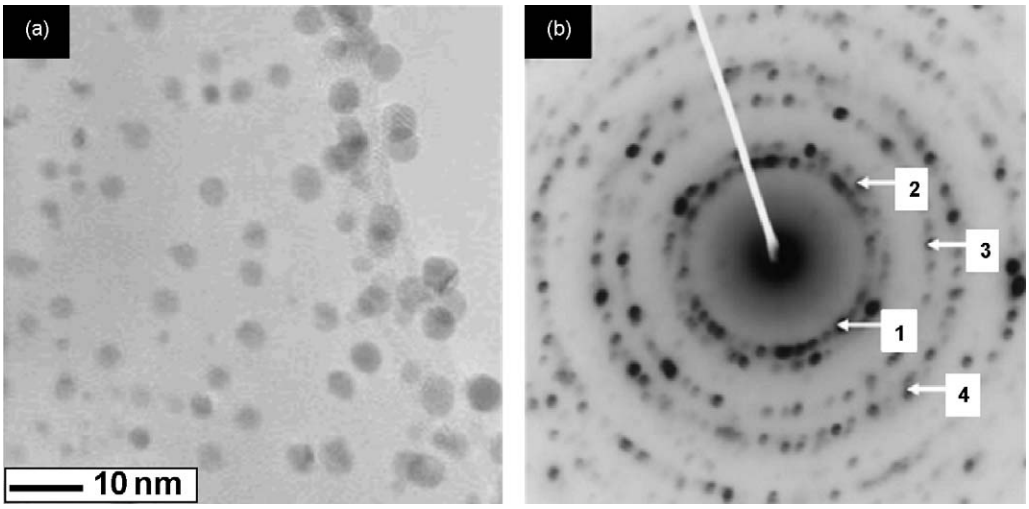

Fig. 3. Representative TEM image of monometallic Au/SA sample (a) and their electron diffraction pattern (b). The rings 1, 2, 3 and 4 diffraction spots are due to the (1 1 1), (2 0 0), (2 2 0) and (3 1 1) reflections of the lattice planes of faced centre cube.

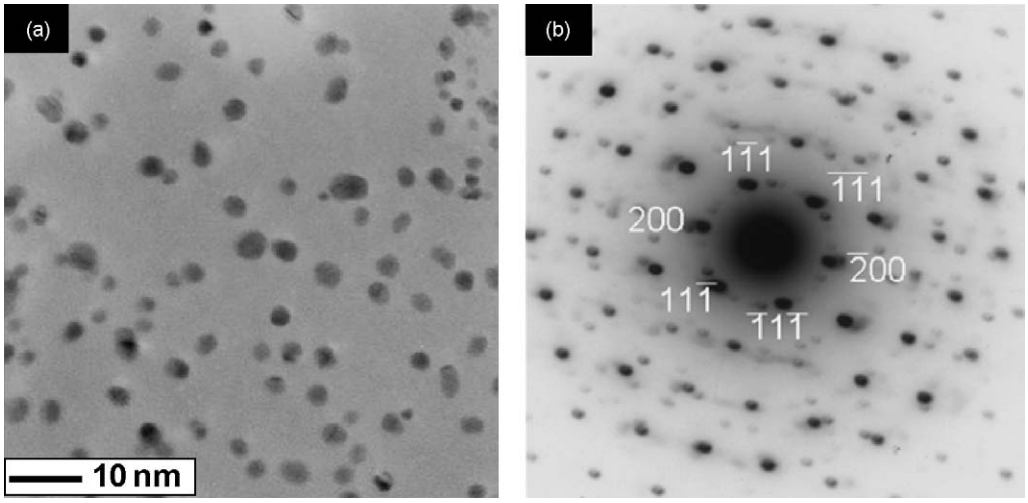

Fig. 4. Representative TEM image of bimetallic AgAu/SA sample (a) and their electron diffraction pattern (b). The diffraction spots are indexed on the basis of the faced centre cube structures.

conduction band electrons that are induced by the incident electromagnetic radiation when the wavelength of the incident light is greater than the particle size [41]. Then, we could expect that the differences observed by DRX and TEM on the morphology and distribution of particle size observed in both monometallic and bimetallic samples were reflected on the width, position and intensity of the surface plasmon, and certainly it was the case. We note important differences of this band between both samples. The plasmon resonance in the spectrum of the monometallic sample is wide and of low intensity. On the other hand, in the bimetallic sample it shows a narrow and intense plasmon resonance band (Fig. 6). The narrow and higher intense plasmon resonance band observed in the bimetallic sample could be an indicative of the presence of higher amount of metallic particles with smaller size and a homogeneous size distribution, in comparison with the monometallic sample. This observation seems to be in agreement with the XRD and TEM results. With these results, we can conclude that higher amounts of nanoparticles are formed in the bimetallic sample, in comparison with the monometallic sample. We could also assume that the silver presence has an important influence on the distribution and dispersion of the supported particles of gold.

3.4. X-ray photoelectron spectroscopy

The XPS technique was used to determine the chemical state of gold and silver species and their relative surface exposure on the surface. The binding energy values of the peak of gold, silver, siliceous, aluminium and surface metals/Si atomic ratio are listed in Table 3. The binding energy (BE) at 103.7 and 75.6 eV are characteristics to the presence of Si^{4+} and Al^{3+} ions in the SA material, respectively. The narrow BE values from Si and Al observed in the spectra of support and catalysts indicates that no changes in the electron environment of the SA material occurs after that the metallic particles were supported. This could be an indicative that there is not a strong interaction between the support surface and the supported metallic particles.

Fig. 7(a) and (b) shows the XPS spectra of the Au 4f and Ag 3d core electron levels catalysts, respectively. The monometallic and bimetallic catalysts show a principal Au $4f_{7/2}$ signal around 83.6 eV, the presence of this signal is associated to the presence of Au^0 nanoparticles (Fig. 7(a)) [42]. An additional signal of minor intensity at 84.5 eV was observed in the monometallic sample (Fig. 7(a)). This signal centred at 84.9 eV could be related to the presence of oxidized Au^{1+} species associated with Au_2O_3 phase

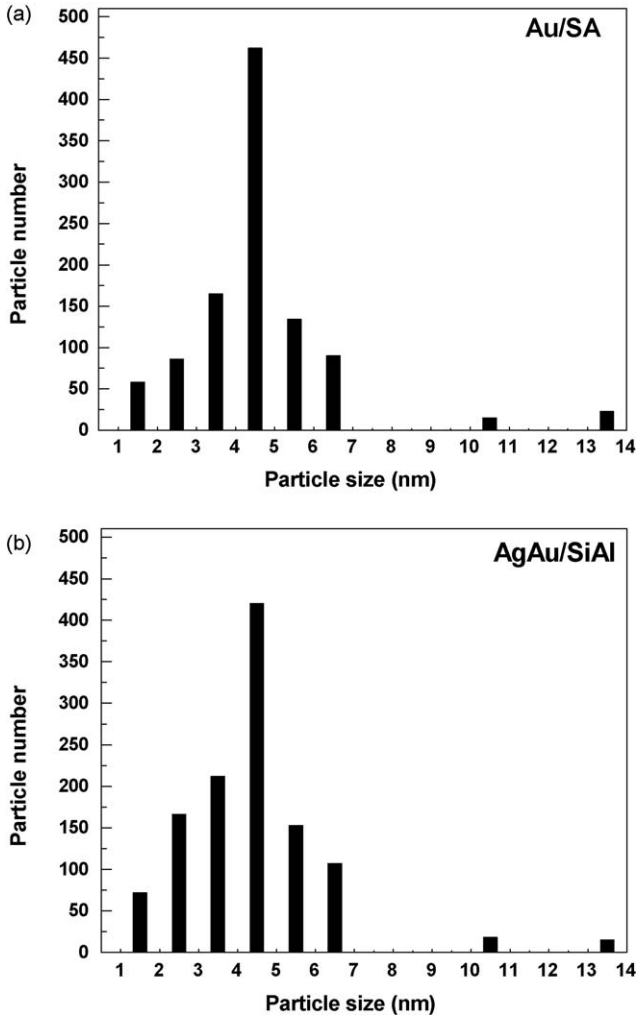

Fig. 5. Particle size distribution corresponds to monometallic Au/SA (a) and bimetallic AgAu/SA (b) catalysts.

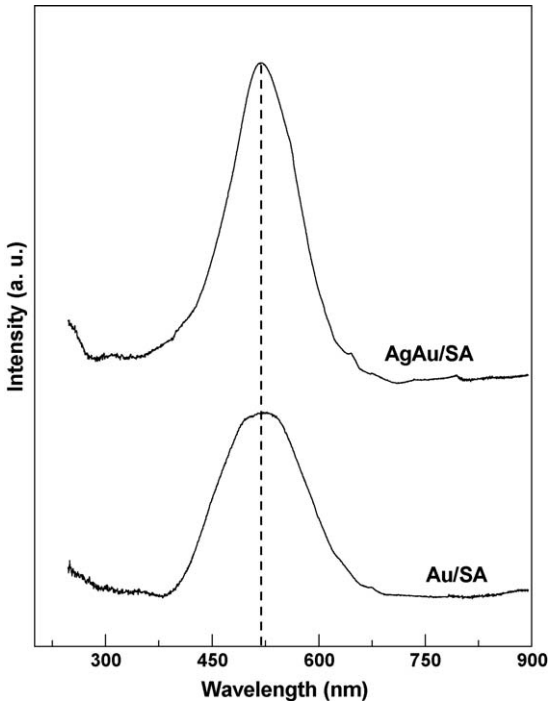

Fig. 6. DRS UV–vis spectra correspond to the catalysts.

Table 3
Binding energies (eV) of core levels and surface atomic ratios of the catalyst.

Sample	Au $4f_{7/2}$	Ag $3d_{3/2}$	Al $2p_{3/2}$	Si $2p_{3/2}$	Au/Si	Ag/Si
SA	–	–	75.7	103.6	–	–
Au/SA	83.6 (81%) 84.9 (19%)	–	75.6	103.7	0.012	–
AgAu/SA	83.6	368.1 (93%) 369.2 (7%)	75.6	103.7	0.006	0.009

[42,43]. We can note that the Au species are completely reduced in the case of the bimetallic sample during the synthesis by the bio-reduction method and also during drying at 100 °C. Contrary to this sample, in the monometallic sample a lower fraction of oxidized Au^{1+} species are presented. Then, we could assume that the presence of silver have multiplex effects on the metallic gold particles, such as: (i) increases the reducibility of the gold species (as observed by XPS), (ii) decreases the size of metallic particle (TEM and DRX study) and (iii) and increment the homogeneity in the size and form of the particles (from the width of the DRS UV–vis and XPS spectra).

The XPS Ag $3d_{3/2}$ peck shows two signals, one at high intensity at 368.1 eV and, the second at lower intensity at 369.2 eV (Fig. 7(b)). The higher intensity signal (368.1 eV) is associated with the presence of metallic Ag^0 particles [44], while the minor XPS signal reveals the presence of Ag^{1+} associated with the AgCl phase [45], as indicated by our XRD results. We can note a higher proportion of metallic Ag^0 species respect to Ag^{1+} species (91 and 9% respectively). In general, we could assume that with the novel bio-reduction method employed in this work it is possible to obtain supported metallic Au and Ag nanoparticles, in a very simple way.

3.5. Catalytic activity

3.5.1. Oxidation of CO

CO oxidation was carried out in a bed quartz micro-reactor, with a feed mixture composition of CO (1%), O_2 (0.5%), N_2 (98.5%) over 150 mg of the catalysts. Catalytic activity results expressed as CO conversion versus reaction temperature over both bio-reduction monometallic and bimetallic samples are shown in Fig. 8. For comparison, in this figure we include the catalytic performance of the Au/SiAl sample (denoted as reference in Fig. 8) prepared by the deposition–precipitation method with similar Au loading and evaluated under same conditions that the others samples. In Fig. 8, we can observe that both bio-reduction samples, shows higher catalytic performance that the Au/SA reference, prepared by the deposition–precipitation method. Both bio-reduction samples show similar initial CO conversion in the temperature range 250–425 K. The ignition temperature at 50% of conversion follows the order: bio-reduction AgAu/SA (435 K) > Au/SA (465 K) ≫ reference Au/SA (540 K). Thus, the bio-reduction AgAu/SA catalyst clearly has a much lower ignition temperature (at 50% of conversion) compared to the other two samples, principally with the sample prepared by traditional deposition–precipitation method. At a reaction temperature of 542 K, 100% of the CO conversion was recorded on bio-reduction bimetallic sample, whereas the CO conversions for the bio-reduction monometallic and reference samples were 85 and 52%, respectively. At the end of the reaction (673 K), the bio-reduction bimetallic sample was 1.15 times more active than their homologous monometallic sample and a 2.27 times superior than the sample prepared by the deposition–precipitation method. Additionally, we can note that both bio-reduction samples showed no catalytic deactivation. In contrast to these two samples, the reference sample showed

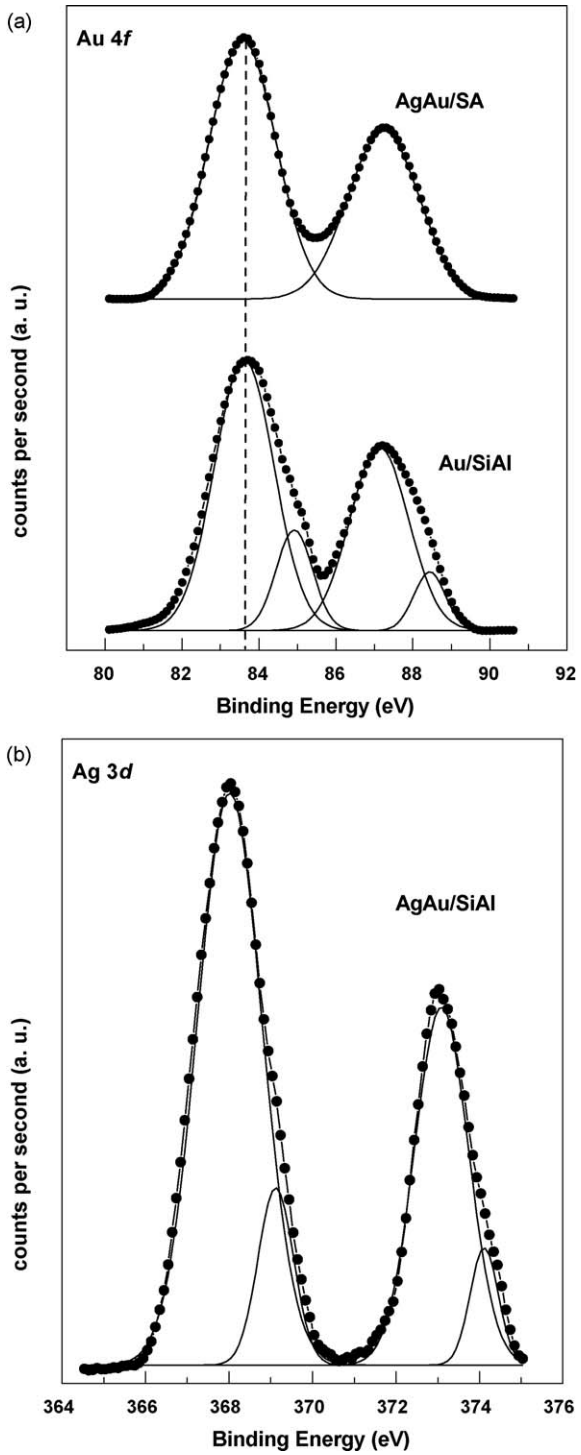

Fig. 7. XPS Au 4f (a) and Ag 3d (b) *core*-level spectra of the catalysts.

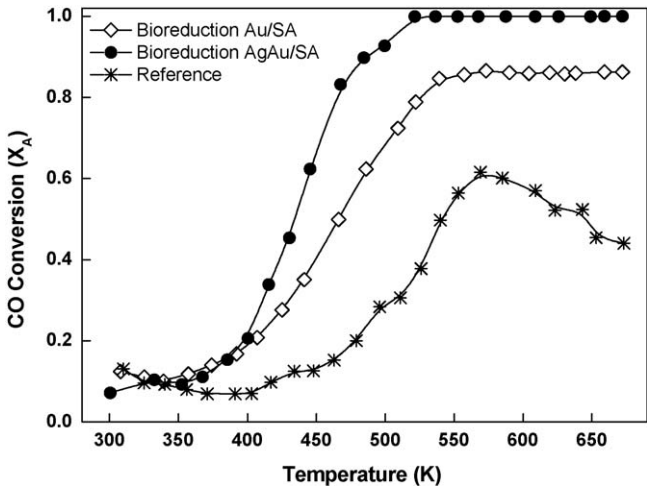

Fig. 8. CO oxidation versus reaction temperature over both bio-reduction Au/SA and AgAu/SA samples and over reference the Au/SA sample (prepared by DP method).

catalytic deactivation under the reactions conditions employed in this works. We could assume that synthesis of Au nanoparticles using the bio-reduction method, resulting in the presence of particles more stable, probably because of the absence of calcinations and reduction procedures employed during the typical synthesis-activation.

Comparing our catalytic activity data, obtaining over ours samples prepared by the bio-reduction method, with different active components supported on pure Al_2O_3 (Al) or on SA prepared by deposition–precipitation method, we could note that ours samples they offer certain advances in comparison with several reports. For example, recently Suo et al. [46], reported the monometallic AuPd/Al prepared by impregnation method, with higher Au loading in comparison with ours catalysts. The authors reported the effect of the calcinations temperature (393, 473, 573 and 673 K) on the CO oxidation test under similar conditions to the reported in this work. The authors found that the sample calcined at 473 K showed higher CO oxidation activity in comparison with the catalysts treated at other temperatures. This sample achieves the 50% of conversion to the 635 K and achieves the 100% of conversion at the 693 K.

Centeno et al. [47], reported the catalytic performance of Au/Al_2O_3 catalyst, prepared by deposition–precipitation with higher Au loading that ours samples (around than two times more) and test under similar conditions to the reported in this work. The author reported the catalytic performance in the CO oxidation of the freshly synthesised samples and of calcination after synthesized samples. The authors reported superior catalytic performance in the CO oxidation over freshly synthesised sample, in comparison with the calcined sample (for 2 h at 773 K in air atmosphere). The freshly synthesised Au/Al_2O_3 sample achievement the 50% of conversion at 593 K reaching the 100% of conversion at 673 K, while the calcined Au/Al_2O_3 sample achievement the 50% of conversion at 753 K reaching the 100% of conversion at 873 K.

Analysing our results with the reported data, we could observe that the use of bio-reduction method employed in the preparation of Au and AgAu catalysts by the CO oxidation, resulting in the obtaining of catalysts with higher activity in this reaction, that then catalysts prepared for deposition–precipitation method.

3.5.2. Hydrogenation of CO

The catalytic performances of bio-reduction catalysts with or without Ag were also tested in the hydrogenation of CO. CO hydrogenation was carried a same reactor that the CO oxidation, but for the CO hydrogenation reaction, we employed a feed mixture composition of CO (1%), H_2 (50%) and N_2 (49%) over 150 mg of the catalysts. The catalytic tests were performances from ambient temperature until 673 K. Fig. 9(a) and (b) shows the catalytic activity in the CO hydrogenation (results expressed as CO consumption) versus reaction temperature over both bio-reduction Au/SA and AgAu/SA samples. For comparison, in Fig. 9(c) we also include the catalytic activity of our reference Au/SA sample prepared by the deposition–precipitation method with similar Au loading. The methane was the only detected product, and the presence of this it was determined by CG-mass spectroscopy (using

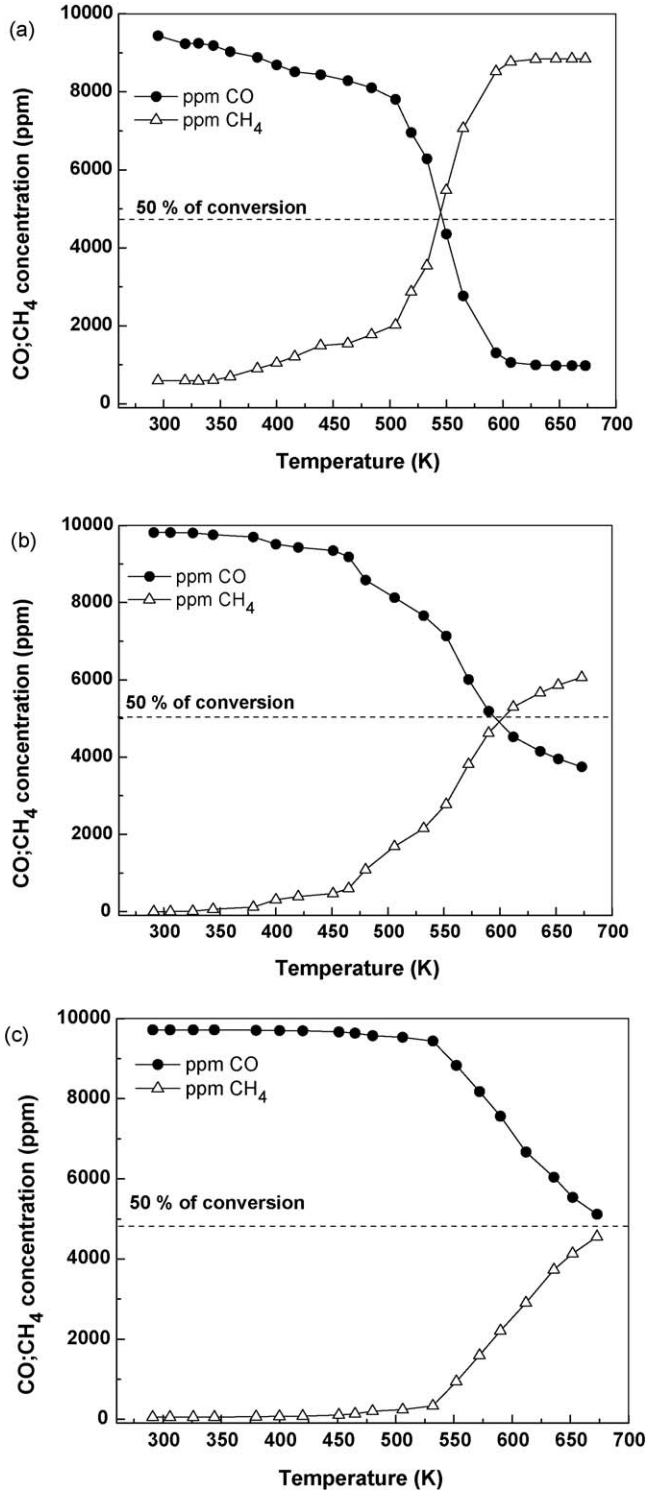

Fig. 9. CO hydrogenation versus reaction temperature over both bio-reduction Au/SA (a) and AgAu/SA (b) samples and over reference the Au/SA sample (prepared by DP method) (c).

a Hidden CG-mass spectrometer model HAL RC 301). The evolution in the methane formation shown in Fig. 9(a)–(c) indicates that the monometallic Au/SA sample prepared by the bio-reduction method has the higher catalytic activity, in comparison with the other two samples. The bio-reduction Au/SA sample reaches a maximum conversion of 92% at 610 K, remaining constant until the end of the reaction. Contrary to this sample, the others two samples, bio-reduction AgAu/SA and reference AgAu/SA samples, both reach a maximum conversion at 673 K, 62 and 47%, respectively. Contrary to the CO oxidation, the monometallic bio-reduction Au/SA sample has the superior catalytic activity, this sample showed 1.6 times more active than the bimetallic bio-reduction sample and a 2 times more active than the reference sample.

Analysing the activity data, we can note that the lower temperature of reaction (540 K) at 50% of CO conversion is observed in the monometallic bio-reduction Au/SA sample. The reaction temperature at 50% of conversion follows the order: bio-reduction Au/SA (540 K) > bio-reduction AgAu/SA (600 K) > reference Au/SA (673 K). Contrary to the CO oxidation, in this reaction, the monometallic samples has the higher catalytic activity in comparison with the others two samples.

We also compared our catalytic activity results for this reaction with some results reported. For example, Panagiotopoulou et al. [4] studied the catalytic performance of Ru, Rh, Pt and Pd catalysts supported on commercial γ-Al_2O_3 during the hydrogenation of CO and CO_2. The authors tested their samples in the CO hydrogenation under similar conditions that we employed in this work. They reported that the selectivity toward hydrogenation products depends strongly on the noble metal used. They found higher catalytic activity and higher methane selectivity over Ru and Rh catalysts than Pt and Pd catalysts. The catalytic activity during CO methanation over both Ru and Rh catalysts initiated at 470 K and the temperature at 50% of conversion is 570 K, getting 100% of conversion at 600 K. The conversion over Pt catalysts is shifted significantly toward higher temperatures, reaching the 50% of conversion at 723 K, whereas the Pd catalyst reached only 12% of conversion at 759 K. The main reaction product with their high activity catalyst (Ru catalyst) was CH_4, however, they reported a lower amount of secondary byproduct such as C_2H_6, C_2H_4 and C_3H_6 which they detected only at temperatures higher than 600 K. Ko et al. [48] reported the selectivity during CO oxidation under the presence of an excess of hydrogen over Au/Al_2O_3, Au/CuO, Au/CeO_2–Al_2O_3 and Au/CeO_2. Catalysts were prepared by the deposition–precipitation method having a similar Au content than that of ours samples. The Au/Al_2O_3 sample reached the 100% CO conversion when the reaction temperature was lower than 335 K, with high selectivity towards CO_2. However, this CO conversion decreased rapidly as the reaction temperature increased further. This could be probably related to the low stability of gold supported particles. Au/CuO sample showed 100% CO conversion when the reaction temperature was 400 K and the selectivity was towards CO_2. Au/CeO_2–Al_2O_3 catalyst showed more than 90% CO conversion at reaction temperature of 493 K, while Au/CeO_2 reached 95% CO conversions at temperature of 573 K, with selectivity to CO_2 over the two last samples. In contrast with the report by Ko et al. [48], the selectivity during CO conversion under the presence of excess H_2 over Au/SA and AgAu/SA was toward the methane formation.

Analysing the performance and selectivity of our Au/SA catalyst with these reported results [4,48], we could then conclude: (i) the synthesis of Au-supported nanoparticles using the one-step bio-reduction method could result in the preparation of effective Au catalysts for the CO hydrogenation and (ii) the Au catalysts prepared by the reported method provides effective catalysts for CO hydrogenation as much as Ru and Rh catalysts and more effective than Pt and Pd catalysts.

Finally, comparing the performance of Au/SA and AgAu/SA catalysts prepared by bio-reduction synthesis method with the performance of the Au/SA sample prepared by DP method, we can concluded that the new on-step bio-reduction method offer important advances and alternatives on the preparation of supported Au and AgAu catalysts in comparison with traditional methods.

4. Discussion

Several reports have showed that the activity of gold catalysts in the oxidation and hydrogenation of carbon monoxide depends strongly on the gold size particles. There are many factors influencing the gold particles size such as preparation method, loading amount of gold and calcinations or reduction temperature [36,49], being the most important factor the gold preparation method. The typical preparation methods for supported nanostructured gold catalysts are the deposition–precipitation and co-precipitation methods (CP) developed until the late 1980s. Several reports have demonstrated that using the above methods is possible to synthesize supported gold nanoparticles smaller than 5 nm. However the solid obtaining after supported gold species by both DP and CP methods is necessary to use the calcination and/or reductions procedures in order to obtain supported metallic Au nanoparticles. Unfortunately, during the calcination and reduction procedures, the sintering and redistribution of the Au species occurs, resulting in the formation of large metallic Au particles with regular morphology and of low energy (electronically very stable).

Under this scenario, one important question arises, (i) it is possible to obtain directly metallic nanostructured Au particles during the deposition of Au species? To give answer to this question, we should revise the recent advances on the novel bio-reduction method for the synthesis of nanostructured metallic noble metals particles [50,51], until today prepared in suspension, and not supported and tested as catalyst. In this study, we reported the synthesis of reduced Au particles in situ during the deposition of the Au species by the novel so-called "bio-reduction" method, using aqueous *C. sinensis* extract. The *C. sinensis* extract contains as main components polyphenols and terpenoids, such as β-cariophyllene (∼0.8 ppm), linalool (∼1.6 ppm), cis-jasmone (∼0.8 ppm), α-terpineol (∼0.8 ppm), δ-cadinene (∼1.7 ppm), indole (∼0.8 ppm), geraniol (∼0.4 ppm), among the major bio-components, which have bactericidal and antioxidant activity, and several other useful properties [52]. These types of compounds contribute to the metal reduction processes, and can also control the size and the stability of the nanostructures formed [53]. The mechanism of nanoparticles formation during the bio-reduction methods may be attributed to the reaction between the metallic ions with hydroxyl as well as carboxylic acid functional groups presents in the bio-compounds of *C. sinensis* extract, whereas the first groups are responsible for the bio-reduction process and the second ones are associated with stabilization and protection as capping agent of the gold nanoparticles [54].

Ours characterization data indicates that synthesis of supported Au and Ag nanoparticles is possible in one-step procedure during the deposition of the metal noble ions on the support surface. The one-step bio-reduction procedure could have several advantages respect to the conventional deposition–precipitation method, such as: (i) the synthesis in one-step of supported metallic metal noble particles, (ii) the synthesis of nanoparticles small size with homogeneous form and (iii) the synthesis of bi-functional Au catalysts for both oxidation and hydrogenation of CO. Comparing the catalytic performance in both hydrogenation and oxidation of CO over the samples prepared by the novel bio-reduction method with the samples prepared by the typical deposition–precipitation method and with the data reported in the references [4,46,47], we can observe superior catalytic activity when the samples are prepared by the bio-reduction procedure. Analysing ours activity data, we can concluded that: (i) the catalysts preparation methods have an important effect on the catalytic performance, (ii) superior performance was observed when the catalysts were prepared by the novel bio-reduction method and (iii) the presence of Ag on the Au/SA system enhances the catalytic performance in the CO oxidation, but the monometallic sample displays superior catalytic performance in the CO hydrogenation.

Even then SA support is not the best for the preparation Au catalysts employed for oxidation and hydrogenation of CO, we can appreciate higher catalytic performance of the samples prepared by the novel bio-reduction method, in comparison with the sample prepared by the deposition–precipitation one. Then, a study on the use of supports such as CeO_2, CeO_2–TiO_2, etc., to the preparation of novel supported Au catalysts for oxidation or hydrogenation of CO could be interesting.

5. Conclusions

This technique of synthesis has yielded nanoparticles with a size distribution in both Au/SA and AgAu/SA samples around 4.5 nm, mainly with a spherical shape. The functional nanostructured materials were tested as catalysts in the carbon monoxide hydrogenation and oxidation reactions showing catalytic activity. The functional nanostructured materials have been proved effectively as catalysts in the hydrogenation and oxidation of carbon monoxide. The bimetallic AgAu/SA sample showed better behaviour in the CO conversion during the CO oxidation process with respect to the other samples. On the contrary, in the case of CO hydrogenation process was the Au/SA monometallic sample which showed superior catalytic performance. This technique to obtain Au and AgAu catalysts supported on SA material, have proved to be uncomplicated, cost effectiveness and environmental friendly, and we expected this approach can be efficient to obtain other nanostructures of noble metals supported, with lower crystal size, homogeneous morphology and high catalytic performance in the reactions involving the CO. It can be conclude that the synthesis of Au and AgAu nanostructures supported on SA material was carried out successfully by a novel, simple and eco-friendly one-step procedure using plant extract as reducing agent.

Acknowledgements

T.A. Zepeda and A.R. Vilchis-Nestor are grateful to CNyN-UNAM and UAM-I (México) for the financial support (Grant IN108908). S.A. Gómez acknowledges the financial support of Consejo Nacional de Ciencia y Tecnología (CONACyT) (Grant 42292). The authors thank F. Ruiz, I. Gradilla and E. Aparicio from CNyN-UNAM for technical support.

References

[1] Z. Kowalczyk, K. Stolecki, W. Rarog-Pilecka, E. Miśkiewicz, E. Wilczkowska, Z. Karpiński, Appl. Catal. A: Gen. 342 (2008) 35.
[2] A.L. Kustov, A.M. Frey, K.E. Larsen, T. Johannessen, J.K. Nørskov, C.H. Christensen, Appl. Catal. A 320 (2007) 98.
[3] F.J. Pérez-Alonso, M. Ojeda, T. Herranz, S. Rojas, J.M. González-Carballo, P. Terreros, J.L.G. Fierro, Catal. Commun. 9 (2008) 1945.
[4] P. Panagiotopoulou, D.I. Kondarides, X.E. Verykios, Appl. Catal. A: Gen. 344 (2008) 45.
[5] D.L. Trimm, Z.I. Önsan, Catal. Rev. 43 (2001) 31.
[6] A.F. Ghenciu, Curr. Opin. Solid State Mater. Sci. 6 (2002) 389.
[7] P.E.H. Nielsen, in: J.R. Jennings (Ed.), Catalytic Ammonia Synthesis: Fundamentals and Practice, Plenum Press, New York, 1991.
[8] G.C. Bond, D.T. Thompson, Catal. Rev. Sci. Eng. 41 (1999) 319.
[9] M. Haruta, N. Yamada, T. Kobayashi, S. Iijima, J. Catal. 115 (1989) 301.
[10] M. Haruta, S. Tsubota, T. Kobayashi, H. Kageyama, M.J. Genet, B. Delmon, J. Catal. 144 (1993) 175.
[11] M. Haruta, Cattech 6 (2002) 102.
[12] V. Aguilar-Guerrero, B.C. Gates, Chem. Commun. (2007) 3210.
[13] O. Pozdnyakova-Tellinger, D. Teschner, A. Wootsch, J. Kröhnert, B. Steinhauer, H. Sauer, L. Toth, F.C. Jentoft, A. Knop-Gericke, Z. Paál, R. Schlögl, J. Catal. 237 (2006) 17.
[14] D. Teschner, A. Wootsch, O. Pozdnyakova-Tellinger, J. Kröhnert, E. Vass, M. Hävecker, S. Zafeiratos, P. Schnörch, F.C. Jentoft, A. Knop-Gericke, R. Schlögl, J. Catal. 249 (2007) 318.
[15] F. Somodi, I. Borbath, M. Hegedus, A. Tompos, I.E. Sajo, A. Szegedi, S. Rojas, J.L.G. Fierro, J.L. Margitfalvi, Appl. Catal. A: Gen. 347 (2008) 216.

[16] R.J.H. Grisel, B.E. Nieuwenhuys, Catal. Today 64 (2001) 69.
[17] G.C. Bond, P.A. Sermon, Gold Bull. 6 (1973) 102.
[18] G.C. Bond, Surf. Sci. 18 (1969) 11.
[19] C. Milone, R. Ingoglia, A. Pistone, G. Neri, F. Frusteri, S. Galvagno, J. Catal. 222 (2) (2004) 348.
[20] B. Pawelec, E. Cano-Serrano, J.M. Campos-Martin, R.M. Navarro, S. Thomas, J.L.G. Fierro, Appl. Catal. A: Gen. 275 (2004) 127.
[21] J.E. Bailie, G.J. Hutchings, Chem. Commun. (1999) 2151.
[22] S. Schimpf, M. Lucas, C. Mohr, U. Rodemerck, A. Brückner, J. Radnik, H. Hofmeister, P. Claus, Catal. Today 72 (2002) 63.
[23] M. Okumura, T. Akita, M. Haruta, Catal. Today 74 (2002) 265.
[24] R. Zanella, C. Louis, S. Giorgio, R. Touroude, J. Catal. 223 (2) (2004) 328.
[25] A.M. Venezia, V. La Parola, G. Deganello, B. Pawelec, J.L.G. Fierro, J. Catal. 215 (2003) 317.
[26] C. Mohr, M. Hofmeister, M. Lucas, P. Claus, Chem. Eng. Technol. 23 (2000) 4.
[27] Y. Zhao, A. Mpela, D.I. Enache, S.H. Taylor, D. Hildebrandt, D. Glasser, G.J. Hutchings, M.P. Atkins, M.S. Scurrell, Stud. Surf. Sci. Catal. 163 (2007) 141.
[28] P. Mohanpuria, N.K. Rana, S.K. Yadav, J. Nanopart. Res. 10 (2008) 507.
[29] R. Joerger, T. Klaus, C.G. Granqvist, Adv. Mater. 407 (2000) 12.
[30] S. Shankar, A. Ahmad, R. Paricha, M. Sastry, J. Mater. Chem. 1822 (2003).
[31] A.R. Vilchis-Nestor, V. Sánchez-Mendieta, M.A. Camacho-López, R.M. Gómez-Espinosa, J. Arenas-A, Mater. Lett. 62 (2008) 3103.
[32] A.Y. Khodakov, A. Griboval-Constant, R. Bechara, F.J. Villain, Phys. Chem. B 105 (2001) 9805.
[33] B. Pawelec, A.M. Venezia, V. La Parolaa, S. Thomas, J.L.G. Fierro, Appl. Catal. A: Gen. 283 (2005) 165.
[34] L. Vradman, M.V. Landau, D. Kantorovich, Y. Koltypin, A. Gedanken, Micropor. Mesopor. Mater. 70 (2005) 307.
[35] T.A. Zepeda, Appl. Catal. A: Gen. 347 (2) (2008) 148.
[36] T.A. Zepeda, T. Halachev, B. Pawelec, R. Nava, T. Klimova, G.A. Fuentes, J.L.G. Fierro, Chem. Mater. 17 (2005) 4062.
[37] P.X. Huang, F. Wu, B.L. Zhu, X.P. Gao, H.Y. Zhu, T.Y. Yan, W.P. Huang, S.H. Wu, D.Y. Song, J. Phys. Chem. B 109 (2005) 19169.
[38] R.Z. Ma, T. Sasaki, Y. Bando, J. Am. Chem. Soc. 126 (2004) 10382.
[39] J.P. Tiwari, C.R.K. Rao, Solid State Ionics 179 (2008) 299.
[40] L.M. Liz-Marzan, Langmuir 22 (2006) 32.
[41] R. Zanella, S. Giorgio, C. Ho Shin, C.R. Henry, C. Louis, J. Catal. 222 (2) (2004) 357.
[42] F. Boccuzzi, A. Chiorino, M. Manzoli, P. Lu, T. Akita, S. Ichikawa, M. Haruta, J. Catal. 202 (2001) 256.
[43] M.M. Mohammed, T.M. Salama, R.O. Ohnishi, M. Ichikawa, Langmuir 17 (2001) 5678.
[44] E. Stathatos, P. Lianos, Langmuir 16 (2000) 2398.
[45] J. Bai, Y. Li, S. Yang, J. Du, S. Wang, C. Zhang, Q. Yang, X. Chen, Nanotechnology 18 (2007) 305601.
[46] Z. Suo, C. Ma, M. Jin, T. He, L. An, Catal. Commun. 9 (2008) 2187.
[47] M.A. Centeno, K. Hadjiivanov, Tz. Venkov, Hr. Klimev, J.A. Odriozola, J. Mol. Catal. A: Chem. 252 (2006) 142.
[48] E.Y. Ko, E.D. Park, K.W. Seo, H.C. Lee, D. Lee, S. Kim, Catal. Today 116 (2006) 377.
[49] R. Zanella, C. Louis, Catal. Today 107–108 (2005) 768.
[50] J. Huang, Q. Li, D. Sun, Y. Lu, Y. Su, X. Yang, H. Wang, Y. Wang, W. Shao, N. He, J. Hong, C. Chen, Nanotechnology 18 (2007) 105104.
[51] S.P. Chandran, M. Chaudhary, R. Pasricha, A. Ahamd, M. Sastry, Biotechnol. Prog. 22 (2006) 577.
[52] T.M. Rababah, N.S. Hettiarachchy, R. Horax, J. Agric. Food Chem. 52 (2004) 5183.
[53] R.P.B. Kaufman, L.J. Cseke, S. Warber, J.A. Duke, H.L. Brielmann, Natural Products from Plants, 1st ed, CRC Press, London and New York, 1999.
[54] K. Yoosaf, B. Ipe, C.H. Suresh, K.G. Thomas, J. Phys. Chem. C 111 (2007) 1287.